Characterizing Fast Arbitrary CW Waveforms With 1500 THz/s Instantaneous Chirps

Ian Coddington, Fabrizio R. Giorgetta, Esther Baumann, William C. Swann, and Nathan R Newbury, *Senior Member, IEEE*

(Invited Paper)

***Abstract*—The instantaneous frequency of a rapidly tuned continuous-wave (CW) laser is measured through linear optical sampling against dual-frequency combs. This dual-comb interferometer determines the instantaneous frequency of the CW laser during a quasi-sinewave frequency sweep of 3 THz amplitude with a 10 ms period. More complicated waveforms are also measured with instantaneous chirps exceeding 1500 THz/s (12 000 nm/s). The uncertainty is 1.5 MHz at 20 ns time resolution, averaging down to 5 kHz at 5 μs time resolution. The absolute frequency accuracy can be calibrated to within 2.5 kHz provided there is a brief period ($<$1 ms) of low laser chirp ($<$160 GHz/s) during the waveform measurement to allow for a dual-comb Vernier measurement of the absolute frequency, modulo 3 THz. This approach allows for the characterization of arbitrary CW waveforms with instantaneous frequencies that change rapidly and over wide optical bandwidth.**

***Index Terms*—Frequency combs, laser tuning, metrology.**

I. Introduction

A FREQUENCY-AGILE, continuous-wave (CW) laser is an ideal source for a range of laboratory and remote-sensing experiments. It can produce a high flux of photons in a single spatial mode allowing for shot noise limited detection with high SNR. Spectral coverage from these devices is limited compared to blackbody sources but still much broader than typical RF sources and growing with advances in lasers. Also, the tuning speed and flexibility of these devices has been increasing [1]–[5]. As CW lasers become more agile, one can envision moving away from the conventional linear-frequency sweep often used with tunable lasers toward more arbitrary CW optical waveforms where the intensity and frequency profile of the laser are tailored for the specific application. For example, in spectroscopy one can dwell on important spectral bands without wasting observation time on the uninteresting intervening spectral regions. In ranging with coherent laser RADAR (LIDAR), one can dynamically tailor the waveform to trade off range resolution with acquisition period depending on the scenario.

Manuscript received November 24, 2010; revised February 2, 2011; accepted February 7, 2011. The work of F. R. Giorgetta was supported by the Swiss National Science Foundation under Grant PBNEP2-127797.

The authors are with the National Institute of Standards and Technology, Boulder, CO 80305 USA (e-mail: ian@boulder.nist.gov; fabrizio@nist.gov; baumann@boulder.nist.gov; swann@boulder.nist.gov; nnewbury@boulder.nist.gov).

Color versions of one or more of the figures in this paper are available online at http://ieeexplore.ieee.org.

Digital Object Identifier 10.1109/JSTQE.2011.2114875

There has been much recent interest in developing fully arbitrary optical waveforms from coherent pulsed sources, i.e., frequency combs [6]–[8]. However, the full implementation of arbitrary optical waveforms remains challenging and the detection equally so. Here, we consider a system to support CW arbitrary optical waveforms, where the term "CW" indicates an intensity and instantaneous laser frequency that are well-defined over the subnanosecond timescales associated with typical high-speed photodetection. There are two obvious challenges to generating CW arbitrary waveforms. First, one must have a CW laser that is capable of achieving the desired waveform. Second, one must be able to accurately control or characterize the optical waveform, in particular the frequency output. (The intensity is easily calibrated with a photodetector.) While a rough calibration of the frequency output is given by the input control parameters used to tune the CW laser, the actual frequency is typically only crudely known compared to the laser linewidth, particularly at high tuning speeds. This paper addresses that second challenge by refining measurement capabilities.

This problem of achieving a known frequency profile has been addressed in a number of different systems that use either active feedback to control the CW laser frequency or passive measurements of the CW laser output [9]–[18]. The active systems avoid the complexity of postprocessing but do require high-bandwidth and high dynamic-range feedback. This level of feedback is not always possible or may restrict possible waveforms. Passive approaches based on monitoring the waveform and correcting for distortions in postprocessing can be more flexible. However, conventional frequency metrology instruments such as optical spectrum analyzers and wavelength meters have nowhere near the necessary combination of speed, resolution, and accuracy. Measurements against etalons or interferometers can provide relative frequency measurements at reasonable resolution and speed but the accuracy is limited by dispersion or thermal/mechanical changes in the reference device. Additionally, the absolute frequency must be determined separately.

Many of the approaches to creating a known frequency profile have exploited frequency combs [9]–[16]. Frequency combs have set new standards for frequency metrology of static CW lasers [19], [20], and it is indeed natural to extend their use to metrology of dynamic CW lasers. The broad spectral output of femtosecond frequency combs provide a high accuracy spectral ruler across a broad bandwidth when properly stabilized to a frequency reference. Early comb work has allowed for

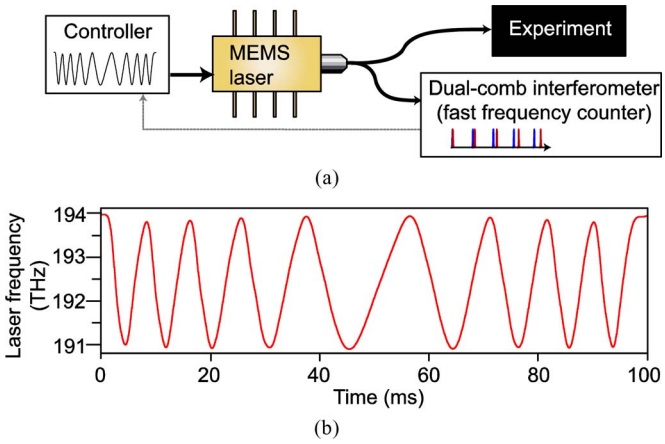

Fig. 1. (a) Schematic of the setup. The laser controller inputs the approximate desired waveform to the MEMS-based tunable CW laser. The output is split with a small portion directed to the coherent dual-comb interferometer that acts as a fast optical frequency counter to measure the actual output waveform. The CW laser is briefly held constant for ∼1 ms to acquire the absolute frequency prior to rapid modulation. (b) Measured frequency swept waveform with a 3 THz peak-to-peak amplitude and a modulation frequency that varies from 125 to 50 Hz. The time resolution is 20 ns. The output waveform only approximately follows the control voltage. The measured waveform can be used in postprocessing of the experimental results or, optionally used to tailor the control voltage, as indicated by the light gray line in (a).

high-resolution active control or passive measurement of CW waveform, but frequency tuning rates have been limited. More recently, in [21] the relative frequency profile of a tuned CW laser was tracked through its successive crossings of comb teeth. Tuning speeds as high as 1 THz/s are possible with this method. In our recent work [22], we used a highly coherent dual-comb interferometer to make rapid, absolute measurements of a CW laser frequency at high time resolution and accommodating frequency sweeps up to 100 GHz/s or 1 THz/s depending on system parameters. An earlier version of the system presented here was also used to provide calibration of a broadly swept laser system at frequency sweeps of 10 THz/s [23].

The goal of the current work is to push the maximum observable tuning speed of the dual-comb interferometer as high as possible by handing off between relative and absolute measurements of optical frequency. We achieve a significant increase in tuning speed by implementing *IQ* (in-phase/quadrature) detection and relying on mode-hop free tuning of the laser. In that case, we require only a short stable period at the start of the waveform for acquisition of the absolute frequency before transitioning to a much more rapid relative frequency measurement. With these modifications, we are able to track lasers changing as rapidly as 1500 THz/s or 12 000 nm/s.

The system is shown in Fig. 1. It consists of a frequency-agile CW laser, in our case a microelectromechanical system (MEMS) based external cavity diode laser [24] that is rapidly tuned by an arbitrary function generator (AFG). We assume that most of the light would be directed to an external experiment requiring high sensitivity over a broad bandwidth. A remaining fraction is diverted toward our dual-comb interferometer, which acts as a fast and high-resolution-frequency counter. The frequency (and intensity) of the swept waveform can be recorded and the experimental data corrected in postprocessing, or potentially,

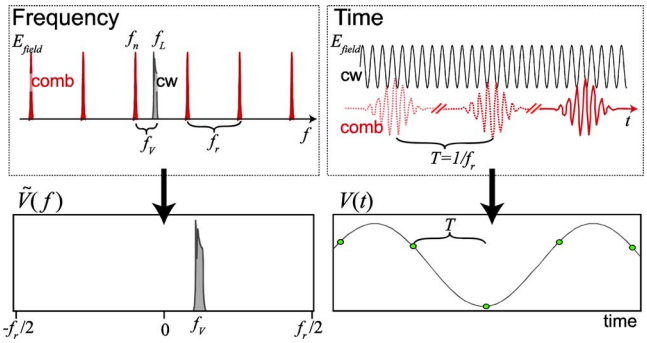

Fig. 2. Simplified picture for frequency metrology of a quasi-static laser (gray) with a frequency comb (red). In the frequency domain (left side), the detected heterodyne frequency, f_V , is the difference between the CW laser frequency, f_L , and nearest tooth frequency, f_n . Similarly, in the time domain (right side), the detected overlap between the comb pulses and the CW laser yields the sampled voltages, $V(t)$, shown as green circles. Ignoring intensity variations, this signal is simply the cosine of the phase difference between the comb pulse and the CW laser at each sampling time.

the measured frequency could be fed back to correct deviations in the waveform. The waveform starts with a brief (<1 ms) stable period so that the dual-comb system can acquire the absolute frequency using our fast coherent implementation [22] of the dual-comb Vernier approach of Ma *et al.* [25] and Peng *et al.* [14]–[16]. After that, the frequency is changed rapidly and tracked through linear optical sampling with a frequency comb. This approach allows us to follow changes in speed and direction of the swept CW laser frequency (unlike the standard approach of tracking crossings of etalon fringes which is consistent with only unidirectional quasi-linear sweeps). We can track tuning speeds exceeding 1500 THz/s and extending over bandwidths in excess of 3 THz. The uncertainty is 1.5 MHz at a 20 ns time resolution and improves linearly with observation time to 5 kHz at 5 μs time resolution. The accuracy of the system is based on the CW reference laser underlying the combs; here, it can be as good as ∼2.5 kHz but might more typically be 100 kHz.

The ability to measure the instantaneous frequency can help characterize the basic behavior of the tunable MEMS laser. We find, as one might expect, that abruptly reaching the edge of the MEMS tuning range results in oscillations in the laser output frequency, presumably because of mechanical resonances. Also, as one might expect, the dc-derived transfer function for the frequency output versus the input control voltages fails to accurately reflect the true high-speed output waveform. Perhaps most promising, and not necessarily expected, we find that the waveforms are quite reproducible over time. Successive waveforms differ by less than 1 GHz, or within the bandwidth of a photodetector. These results indicate it would be possible to "demodulate" the output of one laser with a second tailored waveform. Such capability would allow for ranging at rates much faster than current FM linearly swept LIDAR systems since the demodulated beat could always be tuned to be within a detector bandwidth.

II. Measurement Approach

For metrology of a static CW laser, the comb picture shown in Fig. 2 works well, and the frequency of the heterodyne signal,

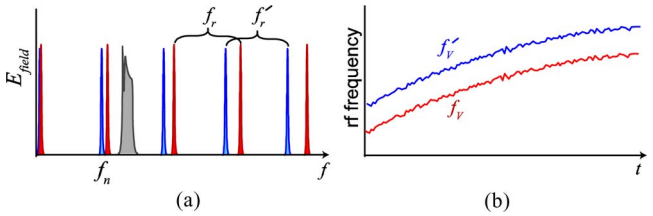

Fig. 3. (a) Simplified picture of the dual combs (red and blue) and the CW laser (gray). (b) Heterodyne signal between the CW laser and nearest pair of comb teeth yields two RF frequencies that vary with time identically, but with a relative offset corresponding to the separation between the comb teeth. This difference can be used to identify the mode number n and thereby yield f_n.

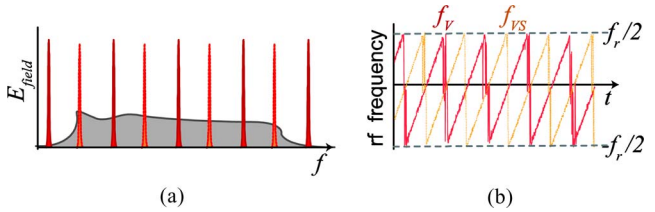

Fig. 4. (a) Simplified picture of the unshifted (red, solid) and shifted (orange, dotted) comb and the swept CW laser spectra (gray, solid). This picture corresponds to a long time window so that the comb teeth are well defined, but the laser frequency has swept over multiple teeth. In practice, we generate a shifted copy of the CW laser rather than the comb, but the principle is the same. (b) Actual measured heterodyne frequencies, f_V and f_{VS} between the unshifted and shifted swept CW laser and the comb. The frequency is always constrained between $-f_r/2$ and $+f_r/2$. The laser frequency is determined by effectively unwrapping the f_V and f_{VS} signals as described in more detail in Section III.B.

$V(t)$, between the CW laser at optical frequency f_L and the nearest comb tooth is

$$f_V = f_L - f_n \tag{1.1}$$

where $f_n = f_{\mathrm{ceo}} + nf_r$ is the frequency of the nth comb tooth, defined in terms of the comb's carrier-envelope offset frequency, f_{ceo}, and repetition rate, f_r. Thus, f_L is known precisely if the comb index, n, is known and if f_{ceo} and f_r are sufficiently quiet. A similar picture can be generated in the time domain, where the comb pulses effectively sample the optical phase of the CW laser at discrete times.

As is clear from Fig. 2, a major challenge with frequency combs is to know which comb tooth one is measuring against, i.e., the value of n in (1.1). We determine n by a Vernier approach using two combs with slightly different repetition rates, f_r and f_r', separated by $\Delta f_r = f_r - f_r'$, as shown in Fig. 3 [14]–[16], [22], [25]. The CW laser is separately heterodyned against each comb yielding RF frequencies, f_V and f_V' that differ exactly by the separation between the nth pair of comb teeth (provided the two combs are optically coherent with each other). It is also worth noting that with IQ detection the sign and magnitude of f_V can be measured.

In the locking scheme shown in Fig. 3(a), this difference, $f_V - f_V'$, is zero at a particular comb index, n_{ref}, whose frequency corresponds to the cavity-stabilized CW reference laser underlying the combs. The frequency difference, $f_V - f_V'$ thus identifies the offset of the tooth index n from n_{ref}, modulo an integer $f_r/\Delta f_r$ (31 883 in our case). After the value of n is calculated from the measured frequency difference, it is adjusted for the ambiguity of $f_r/\Delta f_r$ using *a priori* information on the laser frequency, and then used in (1.1) for an absolute frequency determination.

For this procedure to succeed, one must be able to resolve the difference in the two beat frequencies to better than Δf_r. However, if the CW laser is sweeping very rapidly there may be insufficient time to achieve this level of resolution before the CW laser crosses comb teeth and n is changed. One can still measure the laser spectrum, if an appropriate correction is applied for the laser chirp, as discussed in the supplementary material given in [22]. However, here, we simply will require that the laser tune by less than $f_r/2$ for a period of $1/\Delta f_r$ to determine the comb tooth number.

With the absolute frequency determined, the dual-comb interferometer need only track relative changes (positive or negative) in the laser frequency. This measurement can be made by comparing to a single comb, where we track the now time-varying comb index, $n \rightarrow n\,(t)$, as the CW laser crosses comb teeth. The challenge is to avoid any confusion resulting from the awkward regions where the CW laser lies directly between adjacent teeth and to continuously track the changes in comb index n at ever increasing CW laser tuning speeds.

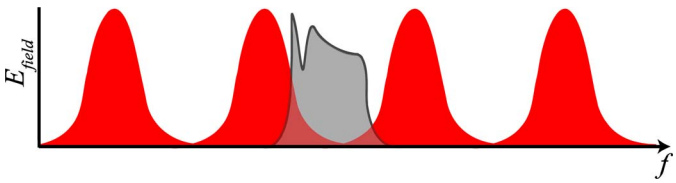

Fig. 5. Spectrum of a CW laser with fast chirp (gray) and a frequency comb (red) over a short period. Over the short period during which the CW laser frequency falls between comb teeth, there are only a few comb pulses and therefore the time-bandwidth-limited comb teeth are quite broad.

The first problems can be solved by a parallel measurement of the CW laser against a second version of the comb, shifted by $f_r/2$, which allows for continuous measurements of the laser frequency through either the heterodyne frequency with the unshifted comb, f_V, or the heterodyne frequency with the shifted comb, f_{VS}, as shown in Fig. 4 [10], [22]; when one heterodyne beat is at a crossing point with an ambiguous frequency of $\pm f_r/2$, the other is at a well-defined frequency near zero. In our implementation, we actually generate a shifted version of the CW laser by an acoustooptic modulator (AOM), but the concept is the same.

The tracking of the mode number of course becomes progressively more challenging as the chirp of the laser frequency $C \equiv \dot{f}_L(t)$ increases. As the interaction period between the swept laser and a single tooth becomes shorter the tooth becomes significantly time-bandwidth limited (as depicted in Fig. 5). Certainly once the laser frequency changes by more than a comb tooth spacing f_r in a period $T = f_r^{-1}$ (i.e., $C > f_r/T$), the interaction of the swept CW laser with a single-comb tooth is not defined as comb teeth are not defined over a single pulse. As a rough upper limit then, we require two samples before the laser crosses between comb teeth giving a limit of $C < f_r^2/2$. This limit is of course closely related to the sampling theorem for nonbaseband measurements.

As the comb picture breaks down for short observation times, it becomes more appropriate to work in the time domain since this avoids subtleties related to the comb formation at short

times, and we can define an instantaneous frequency. As discussed in more detail in the Appendix, from the *I* and *Q* signals, we can extract the phase of the signal $V(t)$ sampled at the kth pulse at time $t_k = k/f_r$. The sampled phase is given by

$$\theta_V(t_k) = \theta_L(t_k) - 2\pi t_k f_{\mathrm{ceo}} - 2\pi k n \tag{1.2}$$

in analogy with (1.1). From the sampled phases, we define an instantaneous frequency from the central phase difference

$$f_V(t_k) \equiv \frac{\theta_V(t_k + T) - \theta_V(t_k - T)}{4\pi T}. \tag{1.3}$$

The central difference, rather than a two-point derivative, avoids distortions at high chirp level and reduces the noise. A similar instantaneous frequency is calculated for the "shifted" measurement, f_{VS}, and it is these frequencies that are graphed in Fig. 4. (The noise seen whenever f_V or f_{VS} reaches $\pm f_r/2$ corresponds to the breakdown in the implicit assumption of (1.3) that the index n is constant across the phase measurements.) As noted in Fig. 4 and discussed in more detail in Section III-B, the laser frequency is then calculated by unwrapping the frequency measurements to retrieve the laser frequency through (1.1). Given this time-domain description, we can calculate a tighter limit on the maximum chirp. We require at least three measurements of the instantaneous frequency to allow for tracking the frequency trajectory between handovers, with each using a three-point central difference calculation. Including the overlap between these calculation, this translates to a requirement that the CW laser frequency falls within a bandwidth f_r for a time $4T$, or a maximum chirp $C < f_r^2/4$. For our values of $f_r \sim 100$ MHz, the limit is $C < 2500$ THz/s. We operate here very close to this maximal chirp.

III. Experiment

A. Experimental Setup

The experimental layout is depicted in Fig. 6. The combs are femtosecond erbium fiber lasers with repetition rates $f_r \sim f_r' \sim 100$ MHz that differ by $\Delta f_r = 3.14$ kHz. Comb spectra are shown in Fig. 7 and overlap the tuning range of the CW laser. To realize the Vernier measurement of the absolute frequency, a high degree of coherence is established between the combs by phase locking two teeth from each comb to two cavity-stabilized CW reference lasers at 1535 and 1560 nm. The combs and the locking process are described in detail in [26]. The 1560-nm reference laser in combination with counted comb repetition rates provides the absolute frequency calibration of the system; the frequency of the 1560 nm laser can be known to 2.5 kHz through calibration against a self-referenced frequency comb. However, for much of the data shown here the calibration is not current and the absolute reference laser frequency is only known to ~100 kHz. This is more than sufficient for most LIDAR or spectroscopy measurements and on the order of most experimental systematics discussed in the Appendix.

The swept CW laser is an MEMS-based tunable diode laser [24]. The laser can be chirped with rates exceeding 2000 THz/s and is controlled by applying voltages to MEMS mirror actuators for coarse tuning and to a piezoelectric transducer (PZT)

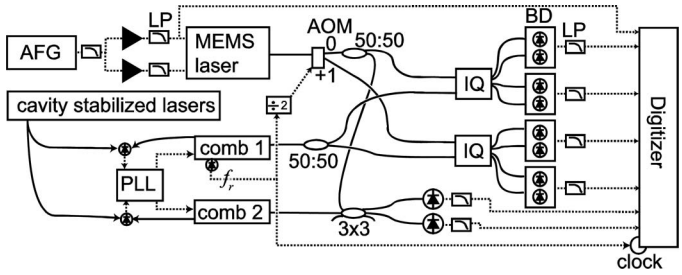

Fig. 6. Experimental layout of the dual-comb interferometer. The output of an AFG is used to generate control signals for the MEMS actuator in the laser (and for the PZT tuning, not shown). The output of the MEMS laser is split, with most of the power being directed toward an external application (not shown) and the remainder to an AOM used to generate a shifted and unshifted version of the CW laser. This light is then sampled by comb 1 using *IQ* demodulators and comb 2 using a 3×3 demodulator followed by BD. A phase-locked loop (PLL) phase locks the combs to a pair of cavity-stabilized CW laser (to provide absolute frequency information). Polarization controllers used to align the polarization into the *IQ* demodulators are not shown. The low-pass filters (LP) are at 150 Hz for the laser control voltages and 50 MHz for the detection channels.

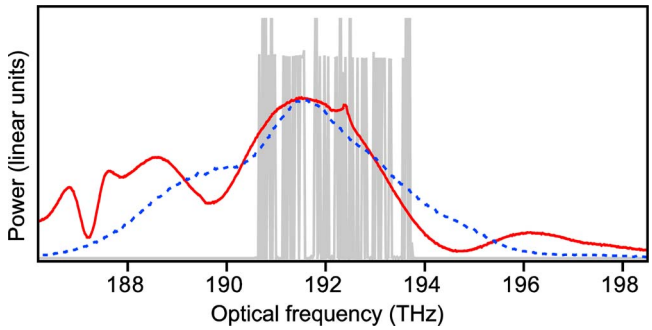

Fig. 7. Normalized spectra of comb 1 (red, solid), comb 2 (blue, dotted) and the swept CW laser (gray). The CW laser is continuously swept, although it appears as discrete lines due to sampling effects in the optical spectrum analyzer.

for fine tuning. For fast sweeps, the PZT is tuned only to prevent mode hops. The control voltage is generated by a 4000-point, 16-bit AFG, and low-pass filtered at 150 Hz to remove bit noise. The filtered signal is passed to three separate high-voltage amplifiers, low-pass filtered again at 150 Hz, and then, applied to both the clockwise and counterclockwise MEMS actuators and to the PZT. By independently tuning the gain and offsets of the three amplifiers, the CW laser can be swept mode hop free over 25 nm (3 THz) centered around 1560 nm.

The CW laser light is directed through an AOM driven with a frequency exactly equal to $f_r/2 \sim 50$ MHz. Both the unshifted and shifted CW light are combined with comb 1 and detected with an optical *IQ* demodulator followed by a pair of 100 MHz-bandwidth balanced detectors, low-pass filtered at 50 MHz to keep the signal within the $\pm f_r/2$ Nyquist bandwidth of the system, and digitized at 12 bits synchronously with f_r. *IQ* detection is particularly helpful, as it removes Nyquist folding effects that can be cumbersome in processing [22]. The resulting in-phase and quadrature voltages are then stored for processing, but it would be possible to implement real-time processing by use of a field-programmable gate array (FPGA). In the processing steps, the *IQ* voltages are first digitally filtered with a 30 kHz to 47 MHz bandpass, and then, normalized to a mean of 0 and a standard deviation of 1. After unwrapping, the arctangent of the

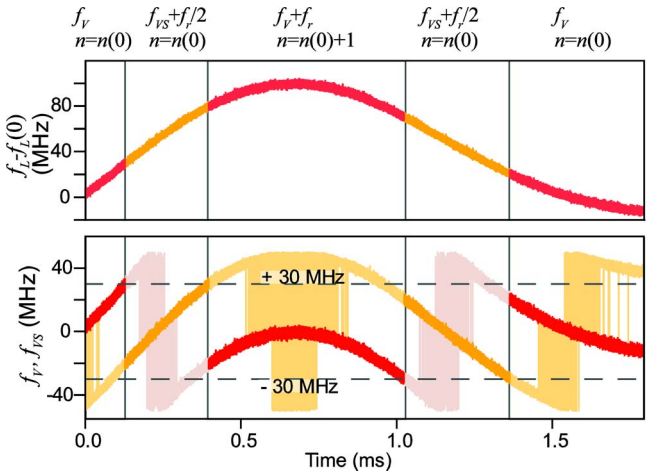

Fig. 8. Hand-off between shifted and unshifted measurement for a slowly tuned laser. (Bottom) Instantaneous RF frequencies for the unshifted measurement, $f_V(t)$ (red), and shifted measurement, $f_{VS}(t)$ (orange). (Top) Calculated instantaneous laser frequency relative to the frequency at $t = 0$, $f_L(t)$–$f_L(0)$, stitched together from $f_V(t)$ and $f_{VS}(t)$ as described in the text and indicated above the figure.

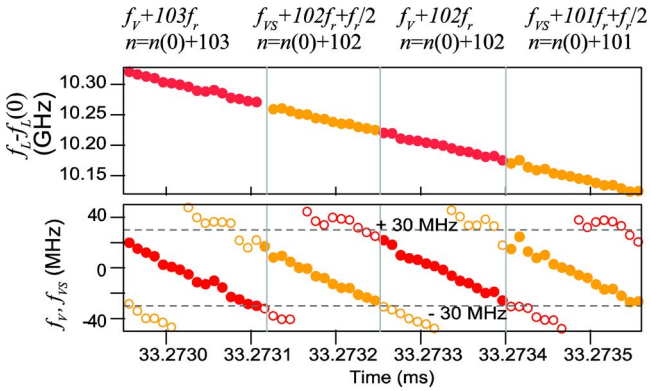

Fig. 9. Hand-off between shifted and unshifted measurement for a rapidly tuned laser at a chirp of ∼800 THz/s but otherwise as in Fig. 8. Data from Figs. 8 and 9 are the data as shown in Fig. 12.

ratio of the normalized in-phase and quadrature voltages yields the instantaneous phase of the CW laser light versus the comb for the unshifted and shifted measurements, θ_V [see (1.2)] and the analogous θ_{VS}, respectively.

The measurement of the CW laser against comb 2 is identical except that a 3×3 coupler is used rather than an *IQ* demodulator (since a third one was unavailable). Two of the output ports of the 3×3 coupler are detected on 100 MHz detectors. The 120° phase shift provided by the 3×3 coupler can be corrected in postprocessing to provide true *I* and *Q* data [27]. The 3×3 approach has the advantage of low price and easy availability; however, the *IQ* demodulators with balanced detection (BD) allowed more power on the detector and a significant increase in SNR.

Because the digitizer is clocked synchronously with comb 1, there is a potential issue with the varying time delay between the clock and the arrival time of the comb 2 pulses. This delay is a problem during periods of high chirp as comb 2 could be delayed by as much as *T*/2, and thus, samples a very different CW frequency than comb 1. If the phase of this varying delay is known, this effect can be corrected in processing. However, we safely ignore this complicating issue as we use only the comb 2 measurement when the chirp is below 160 GHz/s to determine the absolute frequency.

For maximum SNR, we increase both the CW laser power and comb power as high as possible while still avoiding detector saturation. This results in a stronger CW power because the comb pulses saturate the detector at a lower average power. For our commercial balanced detector, powers on each port of the balanced detectors were ∼18 μW of comb 1 light and ∼75 μW of the swept CW laser. The unbalanced detectors each received 20 μW of comb 2 light and 55 μW of the swept CW laser.

Detector saturation will lead to additional measurement noise and systematic error. For the data shown in Figs. 11 and 12, the shifted channel received nearly twice the above power leading to 3 MHz scatter in the data and a 1.5 MHz shift relative to the unsaturated channel at sweeps of 1 PHz/s.

B. Processing

After taking the arctangent of the *IQ* data for the unshifted and shifted measurements against comb 1, we have retrieved $\theta_V(t)$ and $\theta_{VS}(t)$, which are used in (1.3) to calculate $f_V(t)$ and $f_{VS}(t)$. We also obtain the phase samples against comb 2, labeled $\theta'_V(t)$, which are used in (1.3) to calculate $f'_V(t)$. As noted earlier, we first use $f'_V(t)$ and $f_V(t)$ (or $f_{VS}(t)$) over a "quiet" $1/\Delta f_r = 320\ \mu$s window to acquire the absolute laser frequency using the method outlined in Section II [22]. For this period, we require that the laser frequency changes by less than 50 MHz, corresponding to a chirp below 160 GHz/s. The absolute frequency is known modulo the ambiguity of $(f_r f'_r)/\Delta f_r \sim 3$ THz (25 nm) as discussed in Section II. This 3 THz is well within the rough calibration of the laser wavelength versus control voltage. The time window required for the measurement is inversely proportional to the ambiguity; if an ambiguity of 300 GHz is sufficient, the system could be set up such that only a 32 μs time window (or chirp < 1.6 THz/s) is required for the absolute frequency determination. After this absolute calibration, we ignore the $f'_V(t)$ and continuously track the CW laser frequency by "handing over" or toggling the instantaneous frequency calculated from $f_V(t)$ and $f_{VS}(t)$, as outlined in Section II. We assume no mode hops; if one occurs, then the absolute frequency must be reacquired.

We use two different algorithms depending on the chirp. For lower chirps, we simply handover the instantaneous frequency from the unshifted to the shifted measurement (or vice versa) whenever the absolute value of the measured RF signal crosses ±30 MHz. Specifically, when handing over between $f_V(t)$ and $f_{VS}(t)$, we include or remove the factor of $\pm f_r/2$ and increment or decrement the index number *n* as appropriate. This handover is illustrated in Figs. 8 and 9.

At higher chirps ($C > 50$ THz/s), the frequency noise can cause "glitches" of $f_r = 100$ MHz due to either a missed or premature handover of the signal. Therefore we switch to a more predictive algorithm. First, the handover occurs only when the RF signal crosses +30 MHz for a positive chirp and –30 MHz for a negative chirp. Moreover, if the value of $f_V(t)$ (or $f_{VS}(t)$) is just below 30 MHz, it might be that the next value far exceeds

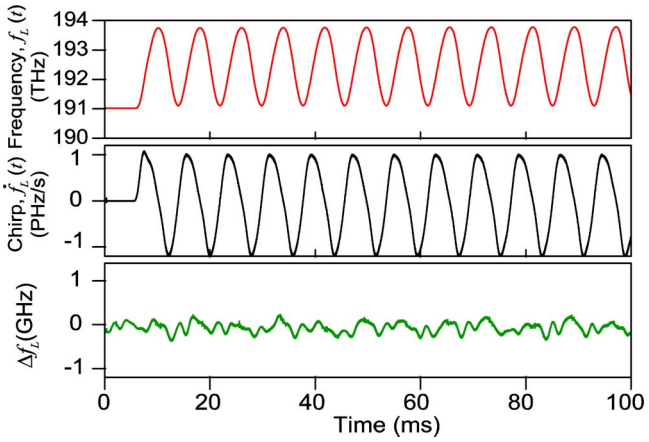

Fig. 10. Example waveform measured for a 125 Hz sinewave modulation applied to the MEMS-based tunable CW laser. The CW laser frequency is plotted at 10 ns intervals. The measurement accuracy is 100 kHz and the uncertainty is ∼1.5 MHz per point using the central difference calculation. It drops linearly with averaging time as shown later in Fig. 14. The brief unswept period at the beginning allows for absolute frequency calibration. The middle plot shows the derivative (chirp), which is boxcar smoothed to a 2 μs resolution. Distortions in the waveform from a true sinewave are evident. Finally, the lower plot shows the maximum deviation observed between 10 successive waveforms over a measurement period of a few minutes. This graph indicates the MEMS-based tunable laser is remarkably reproducible in its output.

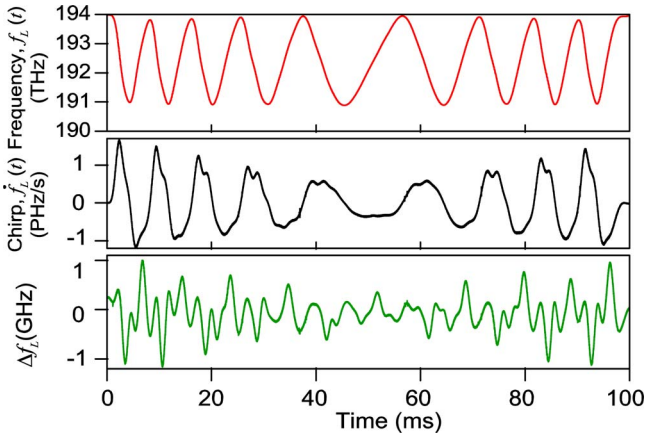

Fig. 11. Example waveform with a 3-THz peak-to-peak amplitude and a modulation frequency that varies from 125 to 50 Hz. As shown in Fig. 10, the top graph is the measured instantaneous laser frequency, the middle graph is the smoothed chirp, and the lower plot is the deviation measured over three successive waveforms. (This waveform is also shown in Fig. 1(b).) The observed structure in the chirp is real and reflects the uneven tuning of the CW laser.

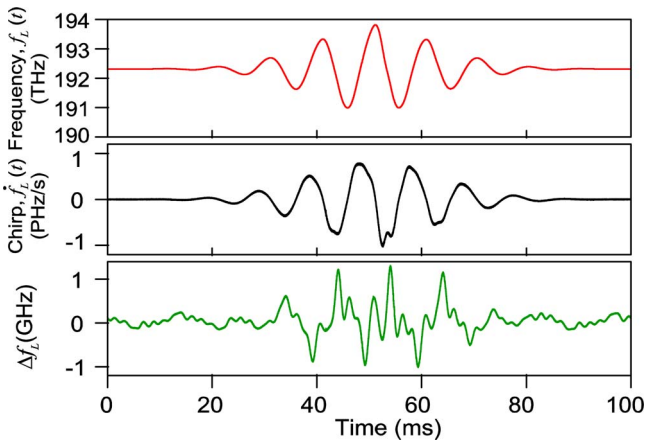

Fig. 12. Example waveform, chirp, and reproducibility for a fixed 100 Hz modulation frequency with varying frequency-modulation amplitude. Other more complex arbitrary CW waveforms can be produced and accurately measured, limited only by the agility of the tunable CW laser and the maximum chirp discussed in the text.

the threshold since (10 ns) × (1500 THz/s) = 15 MHz. Therefore, we project the value of the next frequency $f_V(t)$ and if the projected value exceeds 30 MHz, we anticipate the handover of the signal at the next sample. This handover is illustrated in Fig. 9 for a chirp at half the maximum chirp. This approach dramatically reduces the number of "glitches" that occur. However, on occasion, this simple algorithm can fail at a point resulting in a glitch. This happened at most once in the waveforms shown later in Figs. 11 and 12, and only a few times for Fig. 10, at points of low SNR. The glitches are easily visible and removed by manually unwrapping the frequency by f_r at those points. Since they occur because of a combination of the lower SNR and simple unwrapping algorithm, they could be removed entirely by either a higher SNR or a more sophisticated automated processing. Note the exact value of chirp at which we switch to this predictive algorithm is not critical and can fall anywhere between 10–200 THz/s.

If there is a significant time delay between the effective sampling pulse arrival time, with respect to the CW laser, for the shifted and unshifted channels then the two channels will disagree on the instantaneous frequency for high chirp rates. This will manifest itself as a repetitive frequency shift occurring whenever the unwrapped laser frequency toggles between the shifted and unshifted measurements. We minimize this by adjusting the delays. We verify that this effect is small by comparing $f_V(t)$ and $f_{VS}(t)$ over a time period of strong chirp and find the relative delay to be less than 100 ps or 150 kHz error at a 1500 THz/s chirp. This equivalency between delay and frequency shift is of course, exactly the same as one uses for ranging with a chirped RADAR or LIDAR system. Moreover, this same time offset can in principle be present between the dual comb interferometer measurement and the experiment [see Fig. 1(a)] and must always be measured and properly accounted for.

IV. Results

A. Sweep Data

We demonstrate an array of swept waveforms measured with high fidelity in Figs. 1(b) and 10–13. For these waveforms, the MEMS-based tunable laser was swept over 3 THz in frequency at modulations rates from 50 Hz to 125 Hz. The optical bandwidth was chosen as the maximum mode-hop free range of the laser at these tuning rates and with our control system. The comb spectra roughly matched this bandwidth, as shown in Fig. 7.

We also plot the measured derivative of the waveform, or chirp. From data in Fig. 11, it is clear the dual-comb interferometer can track the laser at chirps exceeding 1500 THz/s (12 000 nm/s).

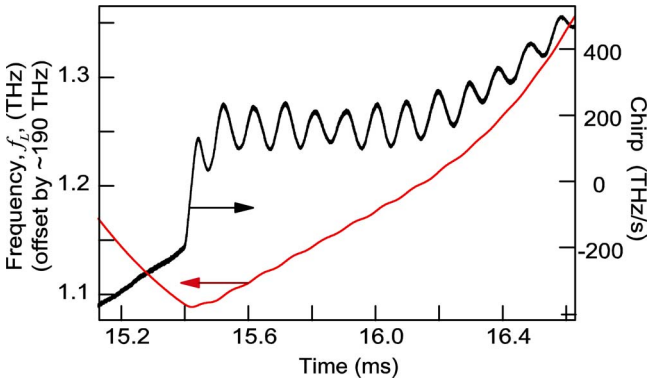

Fig. 13. High resolution and update rate of the system can reveal mechanical effects of the swept laser. The features at 15.4 ms are the response of the swept CW laser as it encounters what is apparently a mechanical stop at the edge of its tuning range.

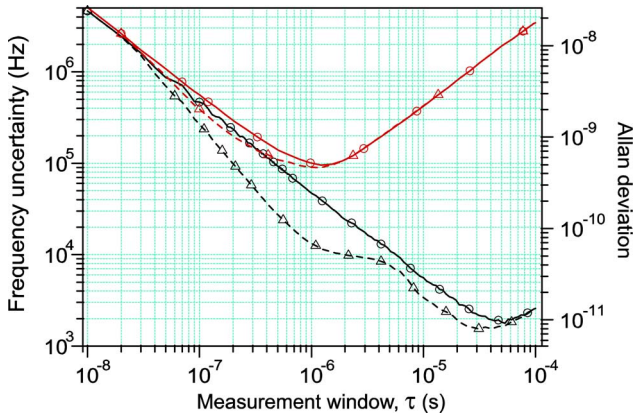

Fig. 14. Allan deviation plot showing the frequency measurement uncertainty as a function of measurement window for the MEMS-based tunable laser (red symbols) and a CW fiber laser (black symbols). The circles show the uncertainty using the two-point frequency determination averaged over a window τ. The triangles show the uncertainty using the multipoint linear phase fit spanning τ.

Finally, we acquired multiple scans using the same arbitrary waveform. The final plot for each waveform shows the maximum frequency deviation, Δf_L, between successive scans. The waveforms are reproducible to 1 GHz, suggesting that one can fairly precisely tailor the waveform of this laser just by pre-adjusting the modulation signal. We note that the deviations for the pure sine waveform are lower than for the other waveforms, presumably because it is a pure tone.

Finally, Fig. 13 shows an expanded view about a time where the MEMS-based tunable laser turns around in frequency after hitting what appears to be a mechanical stop. These data are a simple example of the type of characterization and diagnostics possible given the high frequency and time resolution of the system.

B. Measurement Uncertainty

The central difference method for calculation of frequency [see (1.3)] yields a 1.5 MHz uncertainty in a 20-ns measurement window, dominated by the uncertainty in the individual phase measurements. This frequency uncertainty is a relatively low number for a fast swept laser. However, the instantaneous frequency can be extracted with higher precision given a larger measurement window. One can incorporate more points into the frequency determination by averaging over temporally adjacent frequency or by fitting a line to the time dependant phase. The Allan deviation plot in Fig. 14 shows the measurement uncertainty as a function of time for the unmodulated MEMS-based laser and a quieter CW fiber laser. The frequency uncertainty of the current system is limited by the SNR of the samples, which leads to a ~0.22 rad noise on the measured phases, $\theta_{V\,(\mathrm{VS})}$, and a corresponding $\sim$ 5 MHz uncertainty for a two-point difference calculation of the instantaneous frequency over the 10 ns time between phase measurements. Higher SNR on the phase measurement could be achieved with higher comb power, which is currently limited by detector saturation. Therefore, a higher dynamic range detector or better balancing in the IQ demodulators could allow for an increase in signal and even lower uncertainties. The Appendix discusses other systematic effects when the laser is moving, with the primary contribution arising from group-delay (GD) dispersion in the RF filters.

The uncertainty versus time is characterized by the Allan deviation, which is plotted in Fig. 14 for a two-point phase difference. The two-point method avoids overlapping effects that might distort the Allan curve; however, it yields a slightly higher uncertainty (2.5 MHz over a 20 ns window) than the 1.5 MHz uncertainty of three-point central-difference calculation of (1.3). The uncertainty averages down as $1/\tau$ for the two-point phase derivative technique and slightly faster for an alternate linear phase fit over the same time window (τ). While the MEMS-based CW laser is unmodulated it is not stabilized and at 1 μs the effects of laser drift become apparent as the Allan deviation begins to diverge. A CW fiber laser (also shown) is less prone to drift and one can see the measurement uncertainty average down to 2 kHz.

The method of frequency extraction presented here is different from the FFT based approach presented in [22] in that we measure a center frequency as opposed to a full spectrum. There are a few advantages to this approach that are worth mentioning. First, the method presented here is less processor intensive than an FFT and much more compatible with real-time processing, particularly in an FPGA where processing is naturally point by point. Secondly, this approach accommodates much faster frequency sweeps because instantaneous frequency can be determined to within 1.5 MHz in 20 ns with a single three-point measurement. The drawback of this approach is that one does sacrifice some information. We have reduced all spectral information about the CW laser to a weighted mean frequency, and features such as sidebands or multimodal behavior are largely invisible. Of course, if one is concerned about such effects it is still possible to return to the raw data and perform the FFT analysis.

C. Verification of Accuracy

The absolute frequency accuracy of the system was verified by comparing to measurements made with a self-referenced

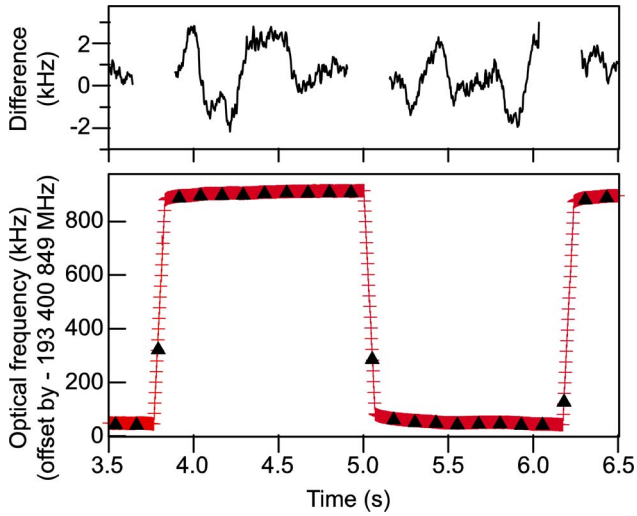

Fig. 15. Absolute-frequency measurements performed with the dual-comb interferometer (red crosses) and a self-referenced comb/wavemeter combination (black triangles).

comb [28] and commercial wavemeter readings to simultaneous measurements made with the dual-comb interferometer. We used an erbium fiber laser with a 1 kHz linewidth in place of the tunable MEMS laser so that the CW laser linewidth would not limit the measurement and to ensure that the laser does not cross a comb tooth during the $\sim$1 s long wavemeter measurement. To synchronize the measurements, the CW laser was modulated with a 1 Hz square wave applied to an intercavity PZT. This modulation periodically shifts the CW laser frequency by 800 kHz. The modulation was much smaller than the wavemeter resolution (10 MHz) and did not affect the readings. During the measurement the heterodyne beat between the CW laser and the self-referenced comb was carefully monitored on a spectrum analyzer to ensure that the tooth number did not change.

Measurements with the dual-comb interferometer were performed as before; however, the slow modulation allows for very-high-resolution measurements. The calibration of the cavity-stabilized lasers underlying the dual-comb interferometer was done immediately prior to the measurement. Measurements made by the two systems are in agreements to within $\pm$2.5 kHz (see Fig. 15). This $\pm$2.5 kHz limit is almost certainly due to unstabilized fiber paths in the experiment [29].

In practice, our absolute accuracy is not 2.5 kHz. The reason is that the frequency of the cavity stabilized reference laser, which we use to calibrate and stabilize our combs, does drift over time. If the reference laser is monitored with a self-referenced comb, as is done for the data in Fig. 15, its frequency can easily be known to a part in 10^1_2. However, for the rest of the data shown here this level of accuracy is unnecessary and the reference laser not continuously monitored. The reference laser drift has been measured at 30 kHz in a day and 100 kHz in a month. For Figs. 10–14, the absolute accuracy of the system is conservatively 100 kHz which is completely sufficient for the measurement. Of course, greater accuracy is achieved with regular calibration of the reference laser or improved temperature stability of the reference cavity. Alternatively, with some increase in complexity one could also perform the dual-comb measurement with self-referenced frequency combs as is done in [14]–[16]. In this case, calibration of the reference laser could be continuous and kHz level accuracy would always be achieved.

It is also worth noting that for fast sweeps it becomes critical to specify where in the system the frequency is being measured as any timing delay is equivalent to frequency shift. At 1.5 PHz/s chirp the CW laser frequency changes 5 kHz over a physical delay of a millimeter. If one were to use the comb system to calibrate a simultaneous gas spectroscopy measurement (see Fig. 1(a)), a difference in paths from the splitting of the CW laser to the point where the signal is recorded would have to be carefully considered. Differential dispersion between one arm of the experiment and the other could also lead to spectrally-dependent errors. For any system needing very high accuracy these timing delay effects would have to be calibrated out. To be clear the dual comb system effectively measures the CW laser frequency at the point where the CW laser and the combs are combined.

V. Conclusion

Dual-comb systems have proven to be capable of high resolution and accurate measurement in both LIDAR [30]–[32] and spectroscopy [26], [33]–[43]. However, the signal-to-noise limitations of these systems make high-SNR rapid measurement difficult [44]. Frequency-agile lasers make an ideal pairing with the dual-comb system providing the resolution and accuracy of the dual-comb system and the sensitivity of a CW laser [22].

We demonstrated a fast, high-precision optical frequency counter based on a dual-comb interferometer. This system can measure the output of a fast swept CW laser with chirp up to 1500 THz/s. Provided there is a brief 320 μs window with a chirp below 160 GHz/s, the absolute frequency is calibrated with an accuracy to better than 100 kHz. Since the maximum chirp scales as the square of the comb repetition rate, higher repetition rate combs [45], [46] could allow for calibration of even faster waveforms.

This system can be used in the laboratory currently to fully characterize the CW waveform from frequency-agile CW lasers. With continued improvements in robust frequency comb sources [47] and with more flexible comb-stabilization techniques [43], one could envision a broadly accessible device or even an arbitrary optical CW waveform generator.

It is also worth noting that combs can access broad regions of the spectrum and one is certainly not constrained to work in the near IR. Therefore, this technique will be compatible with the continued advances in the speed and spectral coverage of agile CW lasers.

Appendix

We evaluate potential systematic errors that might occur at this high chirp due to a number of effects including the approximation of the derivative by discrete samples, variations in the spectral phase of the sampling comb pulses (i.e., chirp in the comb pulses), the low-pass filtering of the detection system, time delays between the two separate measurements of the CW

laser, and shifted CW laser. We do not consider effects of timing delay discussed previously (see Section IV-C).

Assuming a perfectly stable, the comb electric field as a function of time, *t*, is given by

$$E_c(t) = \sum\nolimits_m e^{im\theta_{\rm ceo}} E_P\left(t - mT\right) \tag{1.4}$$

where $\theta_{\rm ceo}$ is the carrier envelope offset (ceo) phase shift [19], [20], $E_p(t)$ is the field of a single pulse, *m* is the pulse number, and *T* is the pulse period. The repetition rate is $f_r = T^{-1}$ and the ceo frequency is $f_{\rm ceo} = f_r\theta_{\rm ceo}/\left(2\pi\right)$. For an input CW laser field $E_L\left(t\right) = \left|E_L\left(t\right)\right|\cos\left(\theta_L\left(t\right)\right)$, the real-valued voltages from the heterodyne beat from the in-phase and quadrature-detection channels are

$$\begin{aligned} V_I(t) &= R(t) \otimes \mathrm{Re}[E_L(t)E_c^*(t)] \\ V_Q(t) &= R(t) \otimes \mathrm{Re}[e^{i\pi/2}E_L(t)E_c^*(t)] \end{aligned} \tag{1.5}$$

where $\otimes$ indicates a convolution with an overall detection response *R*(*t*), which includes the photodetector gain, RF amplifier response, low pass filter, and ADC conversion gain. The *I* and *Q* voltages add to create the complex $V(t) = V_I\left(t\right) + iV_Q\left(t\right)$. Inserting (1.4) into (1.5), this complex voltage is

$$\begin{aligned} V(t) = \sum_m R(t-mT) \int \left|E_L(t)\right| E_P^*(t-mT) \\ \times \exp(i[\theta_L\left(t\right) - mTf_r^{\theta_{\rm ceo}}])dt \end{aligned} \tag{1.6}$$

since *R*(*t*) has a duration much longer than that of the comb pulse, $E_p(t)$. We assume the voltage samples are digitized synchronously with the pulse arrival time to yield a set of complex voltages at times t_k = *kT*. If we assume the detector response is such that *R*(*t*)vanishes for $|t| > T/2$ (we will return to this assumption later), then only one pulse contributes to each digitized signal, and (1.6) gives

$$\begin{aligned} V(kT) = R(0)\left|E_L(kT)\right|\exp(i[-kTf_r\theta_{\rm ceo}]) \\ \times \int e^{i\theta_L\left(t\right)} E_P^*(t-kT)dt \end{aligned} \tag{1.7}$$

for a slowly varying CW laser field intensity. The pulses are very short ($\sim$ ps or less) so the CW laser phase can be expanded as $\theta_L\left(t\right) = \theta_L\left(kT\right) + \left(t - kT\right)2\pi f_L\left(kT\right)$, where the instantaneous laser frequency is defined as $f_L\left(t\right) \equiv \dot{\theta}_L\left(t\right)/(2\pi)$. Equation (1.7) then becomes

$$\begin{aligned} V(t_k) = \left|E_L(t_k)\right|\left|\tilde{E}_P^*(f_L(t_k))\right|R(0) \\ \times \exp(i[\theta_L(t_k) - t_k f_r\theta_{\rm ceo} - \tilde{\theta}_P(f_L(t_k))]) \end{aligned} \tag{1.8}$$

where the Fourier transform of the pulse is $\tilde{E}_P\left(f\right) \equiv \left|\tilde{E}_P\left(f\right)\right|e^{i\tilde{\theta}_P\left(f\right)} \equiv \int E_P\left(t\right)e^{-i2\pi ft}dt$, with spectral phase $\tilde{\theta}_P\left(f\right)$, which might vary slowly across the spectrum if the pulse is chirped. (Note the tilde over the phase indicates only that it is spectrally dependent rather than implying a Fourier transform of the time-dependent phase.) We extract the phase of this signal from the arctangent of the ratio of the real and imaginary components to find

$$\begin{aligned} \theta_V\left(t_k\right) = \theta_L\left(t_k\right) - \tilde{\theta}_P\left(f_L\left(t_k\right)\right) \\ -t_k f_r\theta_{\rm ceo} - 2\pi kn\ + \theta_\sigma\left(t_k\right) \end{aligned} \tag{1.9}$$

or (1.2) with some additional terms.

We have added a term θ_σ to reflect noise on the phase measurement due to detection noise or high frequency phase noise on the combs. For our system, this noise is white and $\langle\theta_\sigma\rangle = 0$. The second-to-last term reflects the fact that the phase could change by any integer multiple of (2π) between measurements and we would be none the wiser. We have specifically chosen the phase offset to be zero for the first sample and to increment by $2\pi n$ between samples; there is no particular reason *n* will be constant and, in fact, it corresponds to the nearest-comb tooth in a frequency picture, so that for a frequency swept CW laser *n* will change. We will require, however, that the value of *n* increments slowly, so that it is at least constant over more than three or four samples. Over this range, we can define the instantaneous measured frequency as in (1.3). We next expand the CW laser phase at time t_k in the Taylor series,

$$\begin{aligned} \theta_L(t) = \theta_L(t_k) + 2\pi(t-t_k)f_L(t_k) \\ +\pi(t-t_k)^2C(t_k) + \frac{\pi(t-t_k)^3}{3}D(t_k) \end{aligned} \tag{1.10}$$

where $f_L\left(t\right)$ is the instantaneous laser frequency, $C\left(t_k\right) = \dot{f}_L\left(t_k\right)$ the instantaneous first-order chirp, and $D\left(t_k\right) = \ddot{f}_L\left(t_k\right)$ the instantaneous second-order chirp. Substituting (1.10) into (1.9) and assuming the integer *n* is constant from $(t_k - T)$ to $(t_k + T)$, the central difference calculation of (1.3) gives

$$f_V(t_k) = f_L(t_k) - f_n - \frac{d\tilde{\theta}_P(f_L)}{2\pi\ df_L}C - T^2D/6 + f_\sigma(t_k) \tag{1.11}$$

where $f_n = \left(f_r\theta_{\rm ceo} + 2\pi nT^{-1}\right)/(2\pi) = f_{\rm ceo} + nf_r$ is the frequency of the $n^{\rm th}$ comb tooth. f_σ is the central difference of θ_σ and leads to the time dependant uncertainty of Fig. 14. For zero comb noise and a constant CW laser frequency $(C = D = 0)$, we have the usual result that the frequency of the heterodyne beat signal, $f_V(t)$, is just the difference between the laser frequency and nearest comb tooth frequency, i.e., (1.1). In the case that $C \neq 0$ or $D \neq 0$ the last two terms could bias the frequency measurement.

The $T^2D/6$ term is deterministic and could be corrected in the data, in principle; however, for our system, the maximum second-order chirp was $D \leq 2\pi(100)C{\sim}2\pi\times10^{17}$ Hz^2/s, so that the correction $T^2D/6 \leq 10$ Hz is insignificant. (Here, and below we have assumed a 100 Hz sinusoidal frequency modulation over a 3 THz bandwidth with a maximal chirp of 1.5 PHz/s.) Note that use of a simple difference between successive samples for the derivative, rather than (1.3), can lead to a more significant correction that is linear in chirp, *C*.

The third-to-last term reflects the interplay of chirp and dispersion in the system. For our system, we estimate that less

than 10 m of single-mode fiber exist from the point that the pulses are time-bandwidth limited to the point where they combine with the CW laser. This fiber will lead to a GD for the pulses, given by the term $(2\pi)^{-1} d\tilde{\theta}_P(f)/df$. A constant GD is no different than the other time delays in the system discussed in the main body of the text. However, a variation of the GD with frequency, i.e., GD dispersion, can cause systematic uncertainty. The GD dispersion of the 10 m of fiber causes a variation of $d\tilde{\theta}_P(f)/df \leq 2\pi\beta_2(10\mathrm{m})(1.5\,\mathrm{THz}) \sim 2\mathrm{ps}$, with a fiber dispersion of $\beta_2 \sim -20$ ps^2/km, giving a maximum systematic uncertainty of (2 ps) $C \sim 2$ kHz. While we have focused on the effect of dispersion on the comb pulse the formalism is identical for the CW laser. Thus, if the CW light is used in a simultaneous experiment, and the paths between the two measurements differ by 10 m of fiber, there would be an equivalent systematic 2 kHz shift over the frequency ramp.

The final important effect that has not yet been included is the low-pass filter in the detector response. The low-pass filter serves two purposes. First, it strongly suppresses the direct detection signal from the comb pulses that occurs at harmonics of f_r. Second, it relaxes the requirements between the synchronicity of the pulse arrival and the clock signal for the digitizer. However, its presence introduces dispersion into the measurement system similar to the fiber dispersion discussed above except that it acts on the RF frequency f_V. The added term to (1.11) is $\delta f_V = (2\pi)^{-1}(d\tilde{\theta}_F(f_V)/df_V)C$, where $(2\pi)^{-1} d\tilde{\theta}_F(f)/df$ is just the GD of the filter. Again, any constant GD is subsumed in the overall time delay of the measurement discussed in Section IV. C, but a variation in the GD, ΔGD, over the 30 MHz range where we utilize the signal can cause systematic shifts. The added uncertainty in the measured heterodyne frequency, and therefore, laser frequency, is $\delta f_V = (\Delta\mathrm{GD})\,C$. For our filters, ΔGD is specified at 2.17 ns, giving a frequency error as large as (2.17 ns)(1.5 PHz/s) = 3 MHz. This is the most significant systematic error we have found, rising just above the point-to-point measurement uncertainty. However, it switches sign as the heterodyne frequency, f_V, crosses zero and should average out for symmetric handover. A flatter phase response for the filter could suppress this effect, or, given that both C and ΔGD can be known quite well, it is probably simplest to remove the error in post processing.

ACKNOWLEDGMENT

Authors would like to acknowledge Z. Barber, K. Knabe, and L. Nugent-Glandorf.

REFERENCES

[1] A. Q. Liu and X. M. Zhang, "A review of MEMS external-cavity tunable lasers," *J. Micromech. Microeng.*, vol. 17, no. 1, pp. R1–R13, 2007.

[2] K. Boylan, V. Weldon, D. McDonald, J. O'Gorman, and J. Hegarty, "Sampled grating DBR laser as a spectroscopic source in multigas detection at 1.52–1.57 μm," *Inst. Electr. Eng. Proc.: Optoelectron.*, vol. 148, no. 1, pp. 19–24, 2001.

[3] V. Jayaraman, Z.-M. Chuang, and L. Coldren, "Theory, design, and performance of extended tuning range semiconductor lasers with sampled gratings," *IEEE J. Quantum Electron.*, vol. 29, no. 6, pp. 1824–1834, Jun. 1993.

[4] J.-O. Wesstrom, G. Sarlet, S. Hammerfeldt, L. Lundqvist, P. Szabo, and P.-J. Rigole, "State-of-the-art performance of widely tunable modulated grating Y-branch lasers," presented at Opt. Fiber Commun. Conf., Los Angeles, CA, Feb. 2004.

[5] R. Phelan, M. Lynch, J. F. Donegan, and V. Weldon, "Simultaneous multispecies gas sensing by use of a sampled grating distributed Bragg reflector and modulated grating Y laser diode," *Appl. Opt.*, vol. 44, no. 27, pp. 5824–5831, Sep. 2005.

[6] S. T. Cundiff and A. M. Weiner, "Optical arbitrary waveform generation," *Nature Photon.*, vol. 4, pp. 760–766, 2010.

[7] Z. Jiang, C. Huang, D. Leaird, and A. Weiner, "Optical arbitrary waveform processing of more than 100 spectral comb lines," *Nature Photon.*, vol. 1, no. 8, pp. 463–467, 2007.

[8] N. K. Fontaine, R. P. Scott, L. Zhou, F. M. Soares, J. P. Heritage, and S. J. B. Yoo, "Real-time full-field arbitrary optical waveform measurement," *Nature Photon.*, vol. 4, no. 4, pp. 248–254, Apr. 2010.

[9] S. E. Park, E. B. Kim, Y.-H. Park, D. S. Yee, T. Y. Kwon, C. Y. Park, H. S. Moon, and T. H. Yoon, "Sweep optical frequency synthesizer with a distributed-Bragg-reflector laser injection locked by a single component of an optical frequency comb," *Opt. Lett.*, vol. 31, no. 24, pp. 3594–3596, 2006.

[10] T. R. Schibli, K. Minoshima, F.-L. Hong, H. Inaba, Y. Bitou, A. Onae, and H. Matsumoto, "Phase-locked widely tunable optical single-frequency generator based on a femtosecond comb," *Opt. Lett.*, vol. 30, no. 17, pp. 2323–2325, Sep. 2005.

[11] J. Jost, J. Hall, and J. Ye, "Continuously tunable, precise, single frequency optical signal generator," *Opt. Exp.*, vol. 10, no. 12, pp. 515–520, 2002.

[12] H. Inaba, T. Ikegami, F.-L. Hong, Y. Bitou, A. Onae, T. R. Schibli, K. Minoshima, and H. Matsumoto, "Doppler-free spectroscopy using a continuous-wave optical frequency synthesizer," *Appl. Opt.*, vol. 45, no. 20, pp. 4910–4915, Jul. 2006.

[13] Y.-J. Kim, J. Jin, Y. Kim, S. Hyun, and S.-W. Kim, "A wide-range optical frequency generator based on the frequency comb of a femtosecond laser," *Opt. Exp.*, vol. 16, no. 1, pp. 258–264, Jan. 2008.

[14] J.-L. Peng and R.-H. Shu, "Determination of absolute mode number using two mode-locked laser combs in optical frequency metrology," *Opt. Exp.*, vol. 15, no. 8, pp. 4485–4492, 2007.

[15] J.-L. Peng, T.-A. Liu, and R.-H. Shu, "Optical frequency counter based on two mode-locked fiber laser combs," *Appl. Phys. B*, vol. 92, no. 4, pp. 513–518, Sep. 2008.

[16] T.-A. Liu, R.-H. Shu, and J.-L. Peng, "Semi-automatic, octave-spanning optical frequency counter," *Opt. Exp.*, vol. 16, no. 14, pp. 10728–10735, 2008.

[17] P. A. Roos, R. R. Reibel, T. Berg, B. Kaylor, Z. W. Barber, and W. R. Babbitt, "Ultrabroadband optical chirp linearization for precision metrology applications," *Opt. Lett.*, vol. 34, no. 23, pp. 3692–3694, Dec. 2009.

[18] N. Satyan, A. Vasilyev, G. Rakuljic, V. Leyva, and A. Yariv, "Precise control of broadband frequency chirps using optoelectronic feedback," *Opt. Exp.*, vol. 17, no. 18, pp. 15991–15999, Aug. 2009.

[19] T. W. Hänsch, "Nobel lecture: Passion for precision," *Rev. Mod. Phys.*, vol. 78, no. 4, pp. 1297–1309, Oct. 2006.

[20] J. L. Hall, "Nobel lecture: Defining and measuring optical frequencies," *Rev. Mod. Phys.*, vol. 78, no. 4, pp. 1279–1295, Oct. 2006.

[21] P. Del'Haye, O. Arcizet, M. L. Gorodetsky, R. Holzwarth, and T. J. Kippenberg, "Frequency comb assisted diode laser spectroscopy for measurement of microcavity dispersion," *Nature Photon.*, vol. 3, no. 9, pp. 529–533, Sep. 2009.

[22] F. R. Giorgetta, I. Coddington, E. Baumann, W. C. Swann, and N. R. Newbury, "Fast high-resolution spectroscopy of dynamic continuous-wave laser sources," *Nature Photon.*, vol. 4, pp. 853–857, 2010.

[23] Z. W. Barber, F. R. Giorgetta, P. A. Roos, I. Coddington, J. R. Dahl, R. R. Reibel, N. Greenfield, and N. R. Newbury, "Characterization of an actively linearized ultra-broadband chirp laser with a fiber-laser optical frequency comb," *Opt. Lett.*, vol. 36, no. 7, pp. 1152–1154, Apr. 2011.

[24] Phoenix1000 MEMS laser data sheet. The use of product names is necessary to specify the experimental results adequately and does not imply endorsement by the National Institute of Standards and Technology. (2009). [Online]. Available: http://www.lunatechnologies.com/products/tunable-laser/files/Phoenix1000_Data_Sheet_2009.pdf.

[25] L. Ma, M. Zucco, S. Picard, L. Robertsson, and R. Windeler, "A new method to determine the absolute mode number of a mode-locked femtosecond-laser comb used for absolute optical frequency measurements," *IEEE J. Sel. Topics Quant. Electron.*, vol. 9, no. 4, pp. 1066–1071, Jul./Aug. 2003.

[26] I. Coddington, W. C. Swann, and N. R. Newbury, "Coherent dual-comb spectroscopy at high signal-to-noise ratio," *Phys. Rev. A*, vol. 82, no. 4, pp. 043817-1–043817-13, Oct. 2010.
[27] C. Dorrer, C. R. Doerr, I. Kang, R. Ryf, J. Leuthold, and P. J. Winzer, "Measurement of eye diagrams and constellation diagrams of optical sources using linear optics and waveguide technology," *J. Lightw. Technol.*, vol. 23, no. 1, pp. 178–186, Jan. 2005.
[28] W. C. Swann, J. J. McFerran, I. Coddington, N. R. Newbury, I. Hartl, M. E. Fermann, P. S. Westbrook, J. W. Nicholson, K. S. Feder, C. Langrock, and M. M. Fejer, "Fiber-laser frequency combs with subhertz relative linewidths," *Opt. Lett.*, vol. 31, no. 20, pp. 3046–3048, Oct. 2006.
[29] N. R. Newbury, P. A. Williams, and W. C. Swann, "Coherent transfer of an optical carrier over 251 km," *Opt. Lett.*, vol. 32, no. 21, pp. 3056–3058, Nov. 2007.
[30] I. Coddington, W. C. Swann, L. Nenadovic, and N. R. Newbury, "Rapid and precise absolute distance measurements at long range," *Nature Photon.*, vol. 3, no. 6, pp. 351–356, Jun. 2009.
[31] N. Tsurumachi, T. Fuji, S. Kawato, T. Hattori, and H. Nakatsuka, "Interferometric observation of femtosecond free induction decay," *Opt. Lett.*, vol. 19, no. 22, pp. 1867–1869, 1994.
[32] M. Godbout, J. D. Deschenes, and J. Genest, "Spectrally resolved laser ranging with frequency combs," *Opt. Exp.*, vol. 18, no. 15, pp. 15981–15989, 2010.
[33] F. Keilmann, C. Gohle, and R. Holzwarth, "Time-domain mid-infrared frequency-comb spectrometer," *Opt. Lett.*, vol. 29, no. 13, pp. 1542–1544, Jul. 2004.
[34] A. Schliesser, M. Brehm, F. Keilmann, and D. Van Der Weide, "Frequency-comb infrared spectrometer for rapid, remote chemical sensing," *Opt. Exp.*, vol. 13, no. 22, pp. 9029–9038, Oct. 2005.
[35] S. Schiller, "Spectrometry with frequency combs," *Opt. Lett.*, vol. 27, no. 9, pp. 766–768, 2002.
[36] T. Yasui, Y. Kabetani, E. Saneyoshi, S. Yokoyama, and T. Araki, "Terahertz frequency comb by multifrequency-heterodyning photoconductive detection for high-accuracy, high-resolution terahertz spectroscopy," *Appl. Phys. Lett.*, vol. 88, no. 24, pp. 241104-1–241104-3, Jun. 2006.
[37] I. Coddington, W. C. Swann, and N. R. Newbury, "Coherent multiheterodyne spectroscopy using stabilized optical frequency combs," *Phys. Rev. Lett.*, vol. 100, no. 1, pp. 013902-1–013902-4, Jan. 2008.
[38] P. Giaccari, J. D. Deschenes, P. Saucier, J. Genest, and P. Tremblay, "Active Fourier-transform spectroscopy combining the direct RF beating of two fiber-based mode-locked lasers with a novel referencing method," *Opt. Exp.*, vol. 16, no. 6, pp. 4347–4365, 2008.
[39] I. Coddington, W. C. Swann, and N. R. Newbury, "Coherent linear optical sampling at 15 bits of resolution," *Opt. Lett.*, vol. 34, no. 14, pp. 2153–2155, 2009.
[40] B. Bernhardt, A. Ozawa, P. Jacquet, M. Jacquey, Y. Kobayashi, T. Udem, R. Holzwarth, G. Guelachvili, T. W. Hänsch, and N. Picqué, "Cavity-enhanced dual-comb spectroscopy," *Nature Photon.*, vol. 4, pp. 55–57, 2009.
[41] I. Coddington, W. C. Swann, and N. R. Newbury, "Time-domain spectroscopy of molecular free-induction decay in the infrared," *Opt. Lett.*, vol. 35, pp. 1395–1397, 2010.
[42] B. Bernhardt, E. Sorokin, P. Jacquet, R. Thon, T. Becker, I. T. Sorokina, N. Picqué, and T. W. Hänsch, "Mid-infrared dual-comb spectroscopy with 2.4 μm Cr2+:ZnSe femtosecond lasers," *Appl. Phys. B*, vol. 100, no. 1, pp. 3–8, Jul. 2010.
[43] J. D. Deschenes, P. Giaccari, and J. Genest, "Optical referencing technique with CW lasers as intermediate oscillators for continuous full delay range frequency comb interferometry," *Opt. Exp.*, vol. 18, no. 22, pp. 23358–23370, 2010.
[44] N. R. Newbury, I. Coddington, and W. C. Swann, "Sensitivity of coherent dual-comb spectroscopy," *Opt. Exp.*, vol. 18, pp. 7929–7945, 2010.
[45] H. Byun, D. Pudo, J. Chen, E. P. Ippen, and F. X. Kärtner, "High-repetition-rate, 491 MHz, femtosecond fiber laser with low timing jitter," *Opt. Lett.*, vol. 33, no. 19, pp. 2221–2223, Oct. 2008.
[46] A. Bartels, D. Heinecke, and S. A. Diddams, "10-GHz self-referenced optical frequency comb," *Science*, vol. 326, no. 5953, pp. 681–681, 2009.
[47] E. Baumann, F. R. Giorgetta, J. W. Nicholson, W. C. Swann, I. Coddington, and N. R. Newbury, "High-performance, vibration-immune fiber-laser frequency comb," *Opt. Lett.*, vol. 34, no. 5, pp. 638–640, Mar. 2009.

Ian Coddington received the B.A. degree in physics from Reed College, Portland, OR, in 1998, and the Ph.D. degree in physics from the University of Colorado, Boulder, CO, in 2004.

He conducted research on Bose-Einstein Condensates at JILA/University of Colorado. From 2005 to 2007, he was an National Research Council Postdoctoral Associate in the Fiber Optics and Components Group, National Institute of Standards and Technology (NIST), Boulder, CO, working toward the development of dual comb spectroscopy in the near-IR and toward coherent frequency transfer. Since then, he has been a Staff Physicist at NIST engaged in the development of dual-comb systems for LIDAR and for monitoring CW and incoherent sources.

Dr. Coddington is a member of the Optical Society of America and the American Physical Society.

Fabrizio R. Giorgetta received the M.Sc. degree in electrical engineering from the Swiss Federal Institute of Technology (ETHZ), Zurich, Switzerland, in 2003, and the Ph.D. degree in physics from the University of Neuchatel, Neuchatel, Switzerland, in 2007, for his work on quantum cascade detectors.

Since 2008, he has been engaged in fiber-laser frequency combs as a Guest Researcher with the National Institute of Standards and Technology (NIST), Boulder, CO.

Esther Baumann received the M.Sc. degree in electrical engineering from the Swiss Federal Institute of Technology (ETHZ), Zurich, Switzerland, in 2003, and the Ph.D. degree in physics from the University of Neuchatel, Neuchatel, Switzerland, in 2007, for her work on photovoltaic light detection in III-nitrides intersubband systems.

Since 2008, she has been engaged in fiber-laser frequency combs as a Guest Researcher with the National Institute of Standards and Technology (NIST), Boulder, CO.

William C. Swann received the B.S. degree in engineering physics from the University of Colorado, Boulder, CO, in 1988.

He was involved in the development of tunable diode lasers and magneto-optical traps for trapping of cesium atoms at JILA/University of Colorado. From 1989 to 1992, he was with DisplayTech, Boulder, CO, developing liquid crystal optical components. In 1992, he returned to JILA, where he worked on optical gyroscope development, as well as fiber-Bragg-grating development. In 1994, he joined Ciena, Baltimore, MD, where he has developed techniques related to production of fiberoptic components for wavelength-division multiplexing (WDM) systems. In 1996, he joined the National Institute of Standards and Technology (NIST), Boulder, where he developed a series of wavelength standards for the optical communications WDM bands. His current research interests include frequency-comb development and applications.

Nathan R. Newbury (M'03–SM'05) received the B.A. degree (*magna cum laude*) from Williams College, Williamstow, MA, in 1986, and the Ph.D. degree in physics from Princeton University, Princeton, NJ, in 1992.

He conducted research on laser-polarized alkali atoms and spin-exchange with noble gas atoms at Princeton University. He was a coauthor of *Princeton Problems in Physics* (Princeton Univ. Press, 1991). From 1993 to 1995, he was a Postdoctoral Associate at JILA, Boulder, CO, working toward the production of Bose–Einstein condensation in laser-cooled atoms. He then joined Lincoln Laboratory, Massachusetts Institute of Technology (MIT), Cambridge, in 1996. In 2001, he joined the National Institute of Standards and Technology (NIST), Boulder, CO, where he is currently working in the area of nonlinear fiber optics and frequency combs.

Dr. Newbury is a member of the Optical Society of America.